SEVENTH EUROPEAN ROTORCRAFT AND POWERED LIFT AIRCRAFT FORUM

Paper No. 9

Modal Characteristics of Rotor Blades - Finite Element Approach and Measurement by Ground Vibration Test

D. Ludwig

DEUTSCHE FORSCHUNGS- UND VERSUCHSANSTALT
FÜR LUFT- UND RAUMFAHRT E. V.
- Aerodynamische Versuchsanstalt Göttingen -
INSTITUT FÜR AEROELASTIK
Federal Republic of Germany

September 8 - 11, 1981

Garmisch-Partenkirchen
Federal Republic of Germany

Deutsche Gesellschaft für Luft- und Raumfahrt e. V.
Goethestr. 10, D-5000 Köln 51, F.R.G.

MODAL CHARACTERISTICS OF ROTOR BLADES - FINITE ELEMENT APPROACH AND MEASUREMENT BY GROUND VIBRATION TEST

D. Ludwig

DEUTSCHE FORSCHUNGS- UND VERSUCHSANSTALT
FÜR LUFT- UND RAUMFAHRT E. V.
- Aerodynamische Versuchsanstalt Göttingen -
INSTITUT FÜR AEROELASTIK
Federal Republic of Germany

Abstract

The mass and stiffness matrices for a rotating blade are established by the finite element method. The formulation is based on the LAGRANGE function presented by J. C. HOUBOLT and G. W. BROOKS for combined flapwise bending, chordwise bending, and torsion of twisted nonuniform rotor blades. The element matrices are created by the non-numeric computer program REDUCE by which it is possible to develop the mathematical model by symbolic manipulation. An ordering scheme was introduced to demonstrate which terms may be simplified or neglected.

As examples, eigenanalyses, with the finite element computer program, are performed for a homogeneous beam and for the non-rotating blade of a wind energy converter. The results of the calculations for the beam are compared with the analytical solutions. The rotor blade of the wind energy converter was tested in a ground vibration test. Thus, it is possible to determine to what extent test results correspond to those of the eigenanalysis. A short description of the ground vibration test technique and performance is given.

1. Introduction

Dynamic stability and response problems of helicopters, wind turbines, and rotary wing aircraft represent some of the most complex problems in aeroelasticity. An important aspect of the aeroelastic investigations of rotating systems is the dynamic behaviour of the rotor blades. Before considering the coupled rotor/fuselage system it must be ensured that there are no snags with the various structural parts.

At the beginning of the aeroelastic analysis, determination of the free vibration characteristics of the rotor blades is an an essential foundation. In the design stage the dynamic behaviour can be determined only theoretically. For this purpose a mathematical model is required representing the main physical properties of the flexible structure. However, the determination of the modal parameters by experiment secures the final dynamic qualification. The free vibration behaviour of the nonrotating blade can be investigated experimentally by a modal survey test.

Considerable work has been done to develop the linear, as well as nonlinear, differential equations of motion for combined flapwise bending, chordwise bending, and torsion of twisted non-

uniform rotor blades. Refs. |1| through |18| represent a typical literature dealing with this topic. In these a great number of cross section constants, which can be determined only with some difficulty, are taken into consideration. The authors specify various reasons as to the importance of these terms and how they are consistent with the fundamental assumptions of the beam theory. This is beyond the scope of this paper.

If one is restricted to the linear analysis, the work of J. C. HOUBOLT and G. W. BROOKS |1| is most usefull. Based on the LAGRANGE function, developed by them, the mass and stiffness matrices for a finite rotor blade element were evolved in Ref. |19|. In it, the assumptions and omissions, which are required to obtain the energy equation, are demonstrated. The analytical deduction was performed by the non-numeric computer program REDUCE. With this program the formulae were derived by symbolic manipulation. In this way a laborious and perhaps faulty manual derivation could be avoided.

The procedure preferred by the Institute for Aeroelasticity of determining experimentally the free vibration behaviour is a modified version of the classical phase resonance method, see Refs. |20|, |21| and |22|. With this method the modal parameters can be measured directly, thus have the advantage that at the end of the tests all free vibration parameters are known and no further calculations are necessary. However, it can be difficult to adapt the excitation to such an extent that in all structural points the phase resonance criterion is satisfied.

2. Basic Assumptions and Kinematics

In order to determine the LAGRANGE function for a rotating beam, geometrical nonlinear theory of elasticity is applied. The nonuniform blade

- is rotating at a constant speed of rotation around the elastic axis,
- is structurally symmetric about the major principal axis,
- can have a built-in twist about the undeformed elastic axis,
- can have an offset from the rotation axis at the hub,
- can have various distances concerning the elastic axis, mass axis and tension axis,
- is of an isotropic material.

It is necessary to introduce an ordering scheme in deriving the equations. This ordering scheme reduces the number of constituent terms and thus not only simplifies the derivation but also it is needed to ignore higher-order terms which do not agree with the basic assumptions. For this purpose all terms are assigned to a certain order, so that the energy equation agrees with those of Ref. |1|. The scheme is used to weight variables for the non-numeric calculation with REDUCE. With this computer program it is possible to neglect the variables in a systematic manner. If terms assigned to the quantity ε are defined to be of first order of magnitude , then terms of an order higher than ε^2 are usually neglected.

The axial coordinate x is of the same order as the rotor radius R. They have the order one and are unweighted as is the

built-in twist β. The coordinates of the cross section η and ζ have the magnitude of the chord and the thickness of the blade, respectively, and are weighted $\varepsilon^{1/2}$. The elastic twist ϕ has the same order. Assuming that the warp function λ is proportional to the product of the chord and thickness, it must be of order ε. The derivatives with respect to η and ζ, respectively, must be of order $\varepsilon^{1/2}$. The elastic displacements in flap and lag direction w and v are weighted with ε. They are of an order less than the axial displacement u. So in consequence the following ordering scheme was used:

$O(1)$: x, R, β, β'

$O(\varepsilon^{1/2})$: $\eta, \zeta, \Phi, \Phi', \Phi'', \lambda_\eta, \lambda_\zeta$

$O(\varepsilon)$: $v, v', v'', w, w', w'', \lambda$

$O(\varepsilon^2)$: u, u', u''.

The elastic deformation of the rotor blade is shown in Fig. 1. The blade is rotating with the X-Y-Z-coordinate system around the Z_I-axis, where Ω is the constant angular velocity. At the hub the blade can have an offcentre distance of e_0. All deformations are referred to the blade-fixed x-y-z-coordinate system, where the x-axis is coincident with the undeformed position of the elastic axis. At an arbitrary point on the blade the ξ-η-ζ-coordinates are attached to the elastic axis. After deformation this system is shifted about the longitudinal displacements u, v, w and rotated about the torsional displacement ϕ.

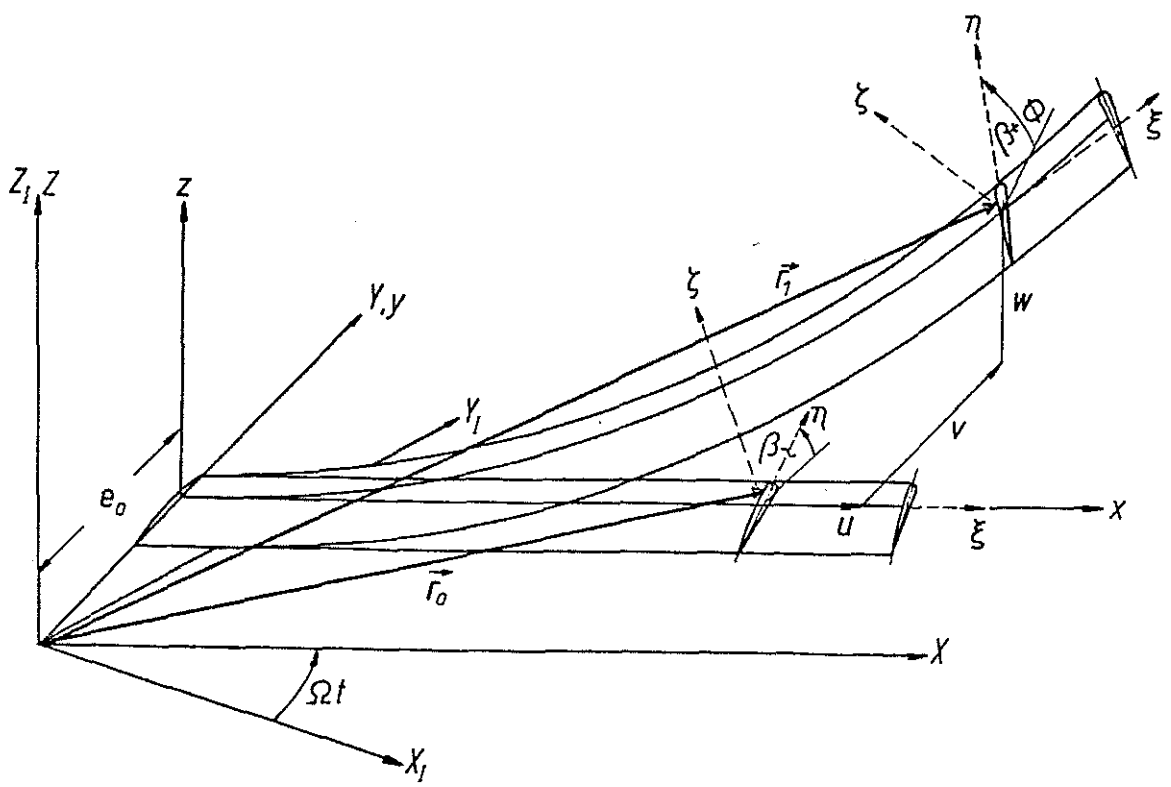

Figure 1: Undeformed and Deformed Rotor Blade

Denoting the position vectors to an arbitrary point of the undeformed and of deformed blade by $\vec{r}_0$ and $\vec{r}_1$, respectively, their corresponding components can be expressed by:

$$(1) \qquad \underline{r}_0 = \begin{bmatrix} x \\ e_0 \\ 0 \end{bmatrix} + \underline{\underline{T}}_0 \begin{bmatrix} 0 \\ \eta \\ \zeta \end{bmatrix}$$

and

$$(2) \qquad \underline{r}_1 = \begin{bmatrix} u + x \\ v + e_0 \\ w \end{bmatrix} + \underline{\underline{T}}_1 \begin{bmatrix} -\lambda\phi' \\ \eta \\ \zeta \end{bmatrix} .$$

The transformation matrices $\underline{\underline{T}}_0$ and $\underline{\underline{T}}_1$ are given in Appendix A.

3. Finite Element Formulation

3.1. LAGRANGE's Equations of Motion

In the case of a holonomic system, the LAGRANGE's equations of motion are expressed in terms of the generalised coordinates q_i and time t as follows:

$$(3) \qquad \frac{d}{dt} \frac{\partial L}{\partial \dot{q}_i} - \frac{\partial L}{\partial q_i} = 0 \qquad i = 1, 2, \ldots, n.$$

The LAGRANGE function L is defined by the difference of the kinetic energy V and the potential energy U:

$$(4) \qquad L = V - U.$$

On the assumption that only stresses due to bending σ_{xx} and due to torsion $\tau_{x\eta}$ and $\tau_{x\xi}$ occur in the rotor blade, the potential energy can be written:

$$(5) \qquad U = \frac{1}{2} \int_0^R \int_A (\sigma_{xx}\, \varepsilon_{xx} + \tau_{x\eta}\, \gamma_{x\eta} + \tau_{x\zeta}\, \gamma_{x\zeta})\, dA\, dx ,$$

where

$$(6) \qquad \sigma_{xx} = E\, \varepsilon_{xx} ,$$

$$(7) \qquad \tau_{x\eta} = G\, \gamma_{x\eta} = 2G\, \varepsilon_{x\eta} ,$$

and

$$(8) \qquad \tau_{x\zeta} = G\, \gamma_{x\zeta} = 2G\, \varepsilon_{x\zeta} .$$

The components of the classical strain tensor ε_{ij} in relation to $\vec{r}_0$ and $\vec{r}_1$, the vector positions of an arbitrary point on the un-

deformed and deformed blade, respectively, can be expressed as:

$$(9) \quad d\vec{r}_1 \cdot d\vec{r}_1 - d\vec{r}_0 \cdot d\vec{r}_0 = 2\,[dx\ d\eta\ d\zeta]\,[\varepsilon_{ij}]\begin{bmatrix} dx \\ d\eta \\ d\zeta \end{bmatrix}.$$

The expression for the kinetic energy of the blade in terms of the velocity of the mass point is given by:

$$(10) \quad V = \frac{1}{2}\int_0^R \int_A \rho\, \vec{v}_1 \cdot \vec{v}_1\, dA\, dx.$$

The vector of the absolute velocity of the mass point $\vec{v}_1$ is defined by:

$$(11) \quad \vec{v}_1 = \dot{\vec{r}}_1 + \vec{\omega} \times \vec{r}_1.$$

The components of the strain tensor and those of the absolute velocity vector are given in Appendix B. In this section the resulting equations for the energy contributions are specified as well.

3.2. Determination of the Finite Element Matrices

Figure 2 shows a typical rotor beam element which has ten degrees of freedom, the two translational motions v and w, and the three rotational motions ϕ, γ and ϑ at each nodal point. The indices "1" and "2" refer to the left and right nodal points, respectively.

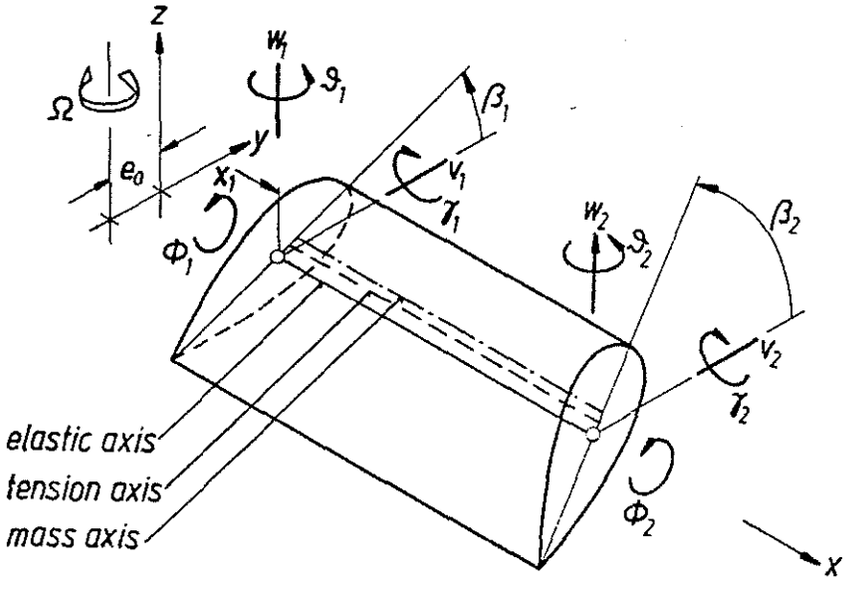

Figure 2: Rotor Beam Element

If the characteristics of the beam element are introduced in the final LAGRANGE's equations of motion, it is possible to calculate the element matrices in relation to the column matrix of the displacements. The integration over the length of one element is performed by REDUCE as are the differentations with respect to the generalised coordinates, their time-dependent derivatives, and time.

For the flap and lag displacements w and v, cubic distributions are assumed. Linear distributions are taken into account for the built-in twist β, for the elastic torsion ϕ, and for the tension T:

$$(12) \quad w = (1 - 3\,\tilde{\tilde{x}}^2 + 2\,\tilde{\tilde{x}}^3)\,w_1 + (3\,\tilde{\tilde{x}}^2 - 2\,\tilde{\tilde{x}}^3)\,w_2 - (\tilde{\tilde{x}} - 2\,\tilde{\tilde{x}}^2 + \tilde{\tilde{x}}^3)\,l\,\gamma_1 + (\tilde{\tilde{x}}^2 - \tilde{\tilde{x}}^3)\,l\,\gamma_2 ,$$

$$(13) \quad v = (1 - 3\,\tilde{\tilde{x}}^2 + 2\,\tilde{\tilde{x}}^3)\,v_1 + (3\,\tilde{\tilde{x}}^2 - 2\,\tilde{\tilde{x}}^3)\,v_2 + (x - 2\,\tilde{\tilde{x}}^2 + \tilde{\tilde{x}}^3)\,l\,\vartheta_1 - (\tilde{\tilde{x}}^2 - \tilde{\tilde{x}}^3)\,l\,\vartheta_2 ,$$

$$(14) \quad \beta = (1 - \tilde{\tilde{x}})\,\beta_1 + \tilde{\tilde{x}}\,\beta_2 ,$$

$$(15) \quad \Phi = (1 - \tilde{\tilde{x}})\,\Phi_1 + \tilde{\tilde{x}}\,\Phi_2 ,$$

$$(16) \quad T = (1 - \tilde{\tilde{x}})\,T_1 + \tilde{\tilde{x}}\,T_2 ,$$

where $\tilde{\tilde{x}}$ is the dimensionless local coordinate in the rotor radius direction.

For one rotor blade element the following parameters are considered as constant:
- distance between elastic axis and tension axis e_A,
- distance between elastic axis and mass axis e,
- distance between elastic axis and rotating axis e_0,
- mass per unit length m,
- mass radii of gyration k_{m1} and k_{m2},
- bending stiffnesses EI_1 and EI_2,
- polar radius of gyration of cross-sectional area effective in carrying tensile stresses k_A,
- torsional stiffness GJ,
- section constants EB_1 and EB_2.

The equations of motion for the beam element can be written in matrix form:

$$(17) \quad \underline{\underline{m}}\,\ddot{\underline{x}} + \underline{\underline{k}}\,\underline{x} = \underline{f} ,$$

where $\underline{\underline{m}}$ is the mass matrix,
$\underline{\underline{k}}$ is the stiffness matrix,
$\underline{x}$ is the column matrix of the nodal point displacements and
$\underline{f}$ is the column matrix of the nodal point forces.

The matrices are symmetric and have the dimension 10 x 10. The column matrices consist of ten elements according to the ten degrees of freedom of the element. If the blade is rotating at a constant angular velocity, then the stiffness matrix is composed of the elastic stiffness matrix and the geometric and centrifugal stiffness matrices. The column matrix of the nodal point forces comprises the column matrices of the tensile and the centrifugal forces.

4. Free Vibration Calculation

In order to calculate the free vibration behaviour of a whole rotor blade, the blade has to be subdivided into a sufficient number of beam elements along the rotor radius. The global matrices are obtained by superimposing the element matrices. Eigenanalysis can be performed for any desired boundary conditions if the desired degrees of freedom are constrained at the hub. Moreover, it is possible to take into account point masses and stiffnesses at the nodal points.

As a numerical example of the free vibration calculation, eigenanalysis of a homogeneous beam was performed. The nonrotating untwisted beam of 2 m length with a rectangular cross section was subdivided into 10, 20 and 40 elements. The first 25 eigenfrequencies and eigenmodes were calculated for the blade which was clamped at the hub.

Within the frequency range of the first 25 eigenmodes lie 13 flap modes, 7 lag modes and 5 torsional modes. In Tab. 1 the natural frequencies of the analytical solution are compared with those computed by the finite element program.

	Analyt.	40 Elements		20 Elements		10 Elements	
Eigenmode	Frequency Hz	Frequency Hz	Deviation %	Frequency Hz	Deviation %	Frequency Hz	Deviation %
1st flap	4.1709	4.1709	-	4.1709	-	4.1710	-
2nd flap	26.139	26.139	-	26.139	-	26.140	-
3rd flap	73.190	73.190	-	73.191	-	73.208	-
4th flap	143.42	143.42	-	143.43	-	143.56	0.1
5th flap	237.09	237.09	-	237.13	-	237.69	0.3
6th flap	354.17	354.18	-	354.30	-	356.08	0.5
7th flap	494.66	494.69	-	495.02	0.1	499.60	1.0
1st lag	16.684	16.684	-	16.684	-	16.684	-
2nd lag	104.56	104.56	-	104.56	-	104.56	-
3rd lag	292.76	292.76	-	292.76	-	292.83	-
4th lag	573.69	573.69	-	573.73	-	574.24	0.1
5th lag	948.35	948.35	-	948.51	-	950.74	0.3
6th lag	1416.7	1416.7	-	1417.2	-	1424.3	0.5
7th lag	1978.7	1978.7	-	1980.1	0.1	1998.4	1.0
1st torsion	179.71	179.72	-	179.75	-	179.89	0.1
2nd torsion	539.13	539.44	0.1	540.37	0.2	544.13	0.9
3rd torsion	898.55	899.99	0.2	904.33	0.6	921.78	2.6
4th torsion	1258.0	1261.9	0.3	1273.9	1.3	1321.9	5.1
5th torsion	1617.4	1625.8	0.5	1651.2	2.1	1752.7	8.4

Table 1: Eigenfrequencies of the Homogeneous Beam

If the length of the elements comprises 5 % of the rotor radius, the results are satisfactory. This means, if the calculation is performed with 20 elements, the frequency deviation is 0.1 % in the 7th flap and in the 7th lag mode. Nearly 2 % deviation was obtained in the 5th torsion frequency. In general, the frequency errors in the torsional modes are high. This is

caused by the linear distribution of the torsional displacements. Since the frequency range of up to 3rd torsion mode of the actual rotor blades is of interest, it is seen from Tab. 1 that the finite element calculations yield good results even with ten elements. The reliability of such calculations depends on the extent to which the structure is subdivided into finite elements.

5. Modal Survey Test on a Rotor Blade

The 50 m rotor blade of a wind energy converter was investigated by a ground vibration test to determine experimentally the modal parameters. Figure 3 illustrates how the blade was clamped to the test setup at the axial coordinate x = 4.3 m. The test stand consists of a stiff steel box connected to a concrete base. The plug for changing the pitch of the blade was mounted on the test setup.

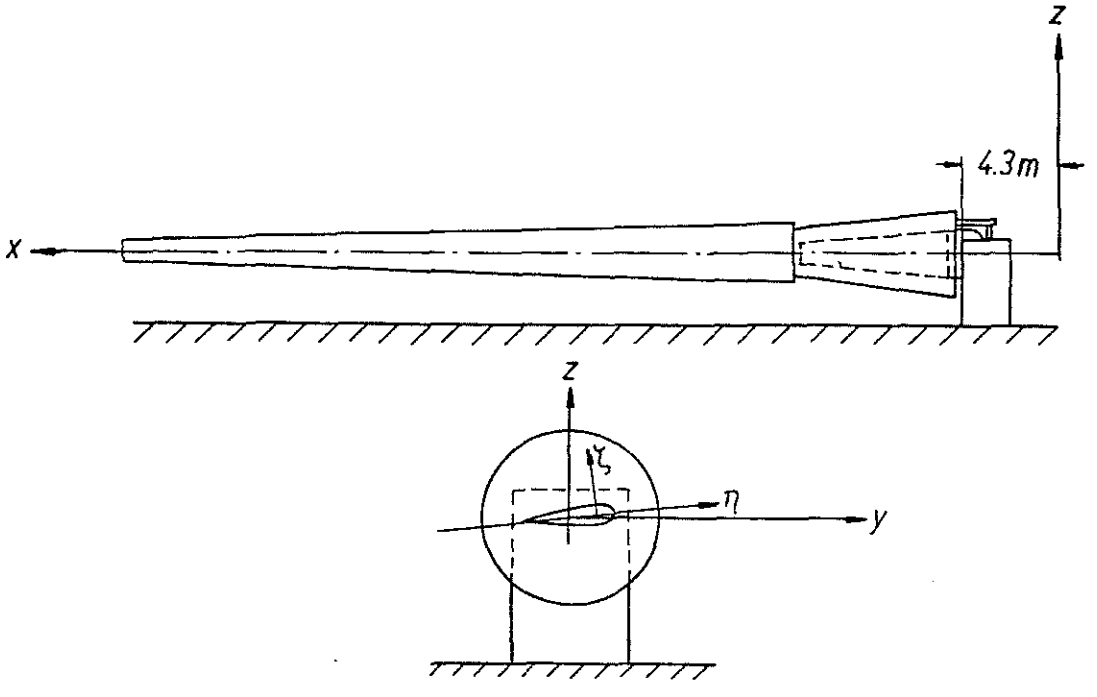

Figure 3: Test Setup

Assuming that the upper limit is the first elastic torsion mode, previous finite element calculations have shown that a frequency range from 0.9 Hz to 26 Hz must be considered. Within this frequency range lie 7 flap modes, 5 lag modes and the torsion mode. For each eigenmode
- the mode shapes,
- the eigenfrequencies,
- the generalised masses and
- the modal damping coefficients

are to be determined.

5.1. Test Procedure

The test was performed with the mobile test assembly of the Institute for Aeroelasticity. Essentially, it is a transportable container, which accommodates the complete data recording equipment including a process computer. This computer-controlled modal survey test technique is based on the phase-resonance method, using a multipoint excitation, to realise the in-phase normal mode condition for all structural points.

It is known that the structural response to a harmonic phase coherent excitation with the circular frequency Ω can be expressed by the uncoupled equations:

$$(18) \quad [-\Omega^2 \bar{M}_r + (1 + i\,\gamma_r)\omega_r^2 \bar{M}_r]\,\hat{q}_r = Q \qquad r = 1,2,3 \ldots m,$$

where M_r is the generalised mass,
ω_r is the circular eigenfrequency,
γ_r is the damping loss angle,
q_r is the complex amplitude of the generalised coordinate and
Q is the amplitude of the generalised force.

The column matrix of the complex geometric displacements $\underline{\hat{X}}$ is to be determined by the superposition of the measured column matrices of the normal modes $\underline{X}_r$:

$$(19) \qquad \underline{\hat{X}} = \sum_{r=1}^{m} \underline{X}_r\,\hat{q}_r .$$

In conformity with the phase resonance method a normal mode exists when there is a phase angle of $\pm\pi/2$ between the dynamic displacements and the excitation forces. For this purpose the excitation frequency and the distribution of the excitation forces must be adapted to the harmonically vibrating structure.

Denoting the real part of the complex $\hat{q}_r$ with q_r' and the imaginary part with q_r'' the phase resonance criterion will be satisfied, if:

$$(20) \qquad q_r' = 0 .$$

Then we obtain for the r-th natural mode shape (referring to the index 0):

$$(21) \qquad -\Omega_0^2 \bar{M}_r + \omega_r^2 \bar{M}_r = 0 ,$$

and

$$(22) \qquad -\gamma_r \omega_r^2 \bar{M}_r q_{r_0}'' = Q_{r_0} .$$

The process of identification of an eigenmode is performed by exciting the structure with slowly increasing frequency and recording the phase resonance criterion with various exciter configurations. The process computer of the test assembly calculates on-line a significant value of the resonance criterion. From the complex acceleration response of all n measuring points

a so-called indicator function Δ is calculated:

$$\Delta = 1000 \left[1 - \frac{\sum_{i=1}^{n} |b_i'| \cdot |b_i|}{\sum_{i=1}^{n} |b_i|^2}\right] . \tag{23}$$

Moreover, the deformations of the structure in terms of the real and imaginary parts of the accelerations can be observed on a display screen. Both the indicator function and the graphic display can be used advantageously in the identification and isolation phase.

For each eigenmode an in-phase vibration must be attempted by means of force and frequency variations. If the phase resonance criterion is satisfied, the exciter frequency is equal to the eigenfrequency and the imaginary parts of the accelerations correspond to the normal mode shapes. In practice, the condition $\Delta \geq 900$ is aimed at in order to obtain sactisfactory modal parameters.

5.2. Test Performance

The rotor blade was excited harmonically by no more than two electrodynamic exciters. There were several points of application of force distributed in rotor radius direction. The metal fittings, provided for the static tests performed after the ground vibration test, were connected with the spar of the blade. These fittings were also used to attach the exciters by tappets. The response of the blade was measured by a number of accelerometers distributed over the blade. Some additional measuring points were arranged at the steel box to control the displacements of the test setup.

The generalised mass of each natural mode shape was computed with the column matrix of the measured eigenmodes $\underline{X}_{r,M}$ by:

$$\overline{M}_r = \underline{X}_{r,M}^T \underline{\underline{M}} \underline{X}_{r,M} , \tag{24}$$

where $\underline{\underline{M}}$ is the mass matrix of the rotor blade based on the physical displacements.

The modal damping coefficients were measured by means of the decay curves. For this purpose the excitation of the structure, vibrating in an eigenmode, was switched off and the response of one accelerometer was recorded. In the case of low damping the loss angle is given by:

$$\gamma_r = \frac{\delta_r}{\pi} \quad 100 \ [\%] , \tag{25}$$

in which δ_r is the logarithmic decrement,

$$\delta_r = \ln \frac{b_j}{b_{j+1}} . \tag{26}$$

6. Comparison of the Test Results with the FE-Calculation

The measured and calculated eigenmodes of the first three flap and lag modes and of the torsion mode are presented in Figs. 4 to 10. In these figures the flap, lag and torsion components are plotted versus the elastic axis. The eigenmodes are normalised such that the generalised mass of each mode shape is unity. Before deviding the test data into the particular components along the elastic axis, a balancing calculation was performed to eliminate measurement errors and to smooth the curves.

The natural frequencies of the calculated modes are always greater than the measured ones. Whereas the lag frequencies agree quite well with the calculations, there is some deviation in the flap frequencies and in the torsion frequency. The maximum deviation is in the torsion mode and amounts nearly 21 %.

The essential difference in the mode shapes which can be observed is the lack of coupling between the flap and lag components in the calculated eigenmodes whereas, there is sometimes a noticeable coupling in the measured mode shapes. The flap and lag frequencies of adjoining measured eigenmodes lie closer together so that coupling is possible. Furthermore, it is obvious that the vibration nodes of the calculated modes are situated closer to the tip of the blade. This may be influencend by the test stand which is not as perfectly stiff as calculated. The accelerometers controlling the displacements of the clamping device indicate small signals, but these were within the range of the test precision.

An orthogonality test with the calculated and measured normal modes and the mass matrix of the FE-calculation was performed. A symmetric correlation matrix of the generalised masses can be determined with a modal matrix composed of the calculated modal matrix $\underline{\underline{X}}_C$ and the measured matrix $\underline{\underline{X}}_M$:

$$(27) \qquad \begin{bmatrix} \bar{\underline{\underline{M}}}_{CC} & \bar{\underline{\underline{M}}}_{CM} \\ \underline{\underline{M}}_{MC} & \underline{\underline{M}}_{MM} \end{bmatrix} = \begin{bmatrix} \underline{\underline{X}}_C^T \\ \underline{\underline{X}}_M^T \end{bmatrix} \left[\underline{\underline{M}}\right] \left[\underline{\underline{X}}_C \; \underline{\underline{X}}_M\right]$$

The submatrix $\bar{\underline{\underline{M}}}_{CC}$ is the generalised mass matrix of the calculated eigenmodes and must be a unit matrix. The submatrix $\bar{\underline{\underline{M}}}_{MM}$ of the generalised masses of the measured mode shapes is a symmetric matrix in which small off-diagonal elements, caused by measurement errors, can occur. The correlation of the calculated and measured eigenmodes can be determined from the matrix $\bar{\underline{\underline{M}}}_{MC}$.

The three submatrices of the correlation matrix are presented in Tab. 2, where all elements are multiplied by 100. In this way, the orthogonality of the measured eigenmodes can easily be determined from the off-diagonal elements of the matrix $\bar{\underline{\underline{M}}}_{MM}$ as percentage. There is rather a substantial deviation of 19 % in the 5th lag mode (L5) which is not quite orthogonal to the 4th lag mode (L4). The 7th flap mode (F7) was measured with nearly 15 % deviation in orthogonality to the 3rd flap mode (F3). For the other mode shapes the orthogonality test yields good results. This is also proved by the high values of the indicator function. These values are arranged in the last column behind the corresponding eigenmode.

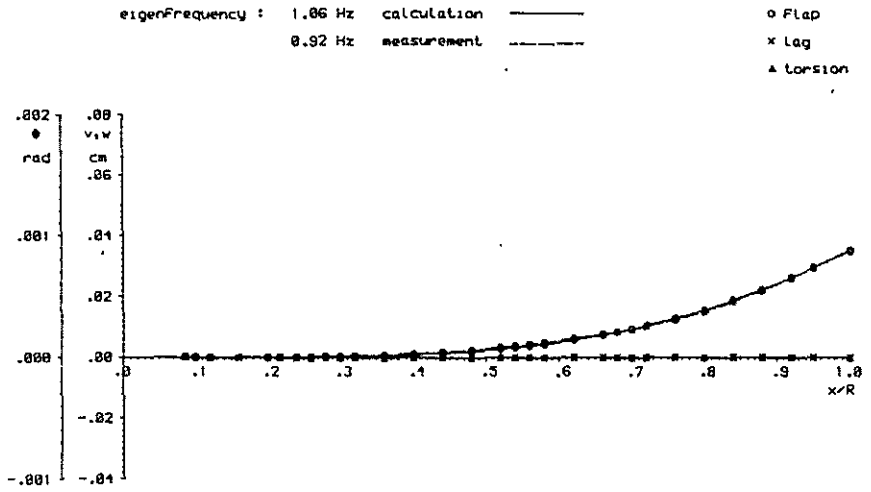

Figure 4: 1st Flap Mode of the Rotor Blade

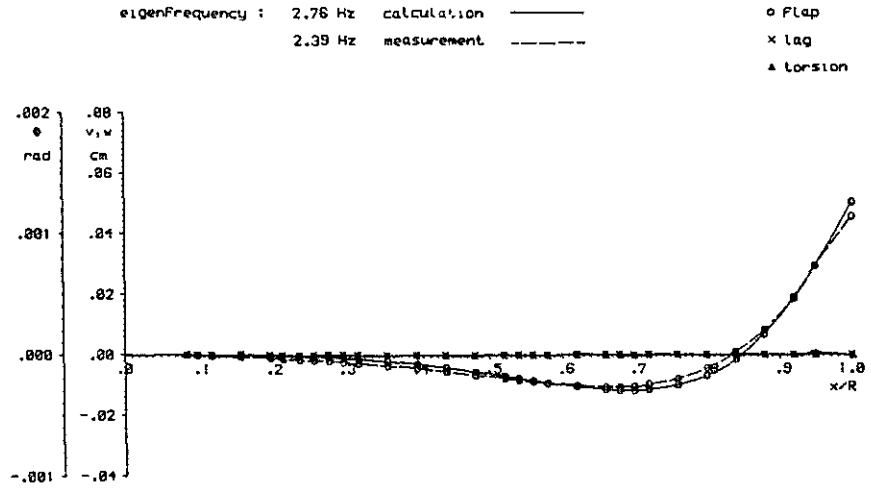

Figure 5: 2nd Flap Mode of the Rotor Blade

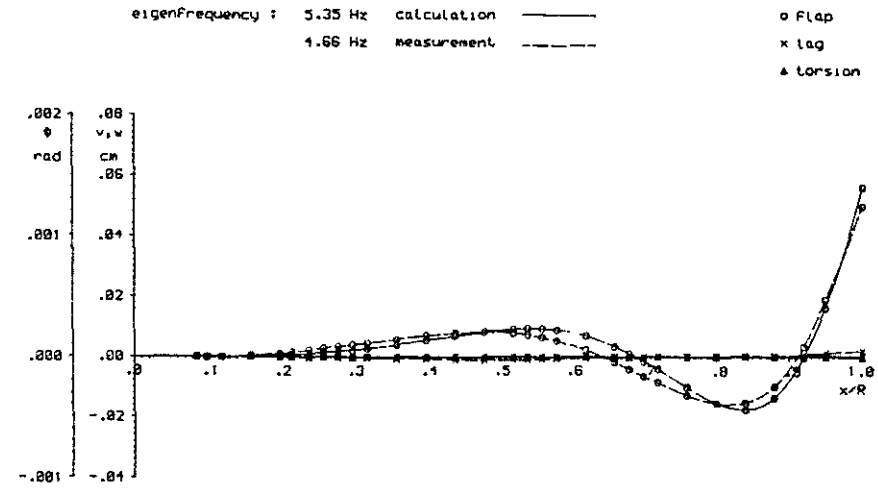

Figure 6: 3rd Flap Mode of the Rotor Blade

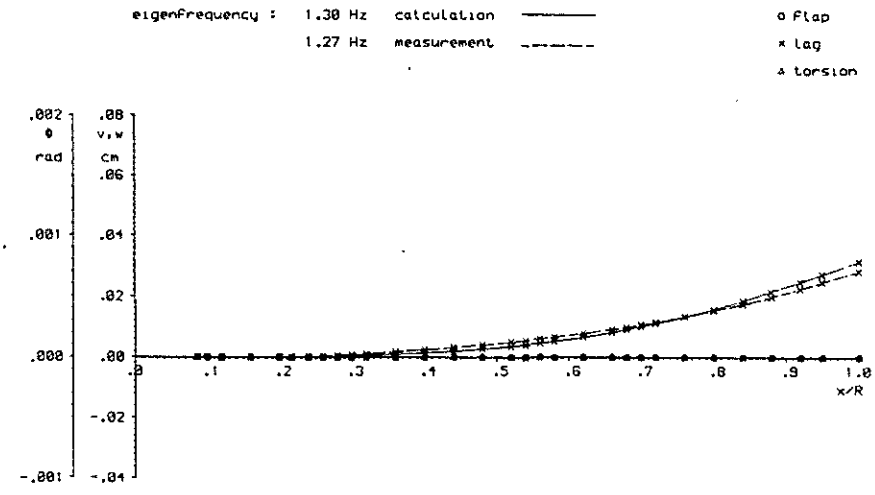

Figure 7: 1st Lag Mode of the Rotor Blade

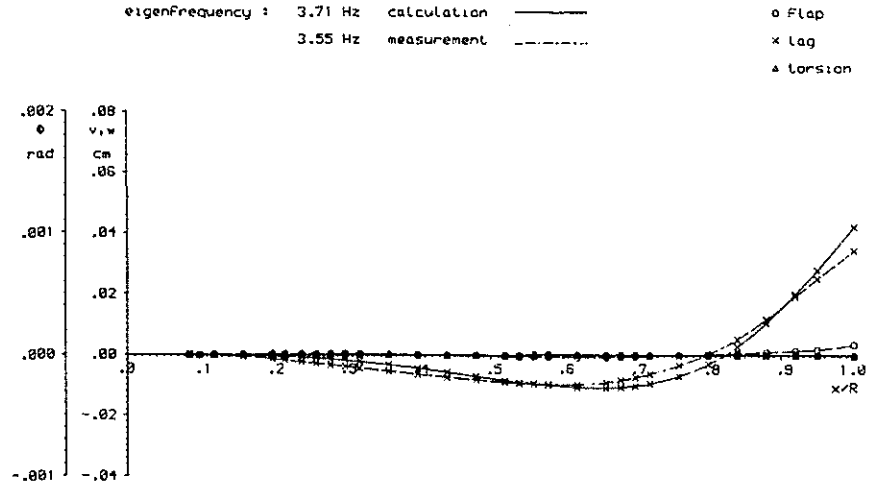

Figure 8: 2nd Lag Mode of the Rotor Blade

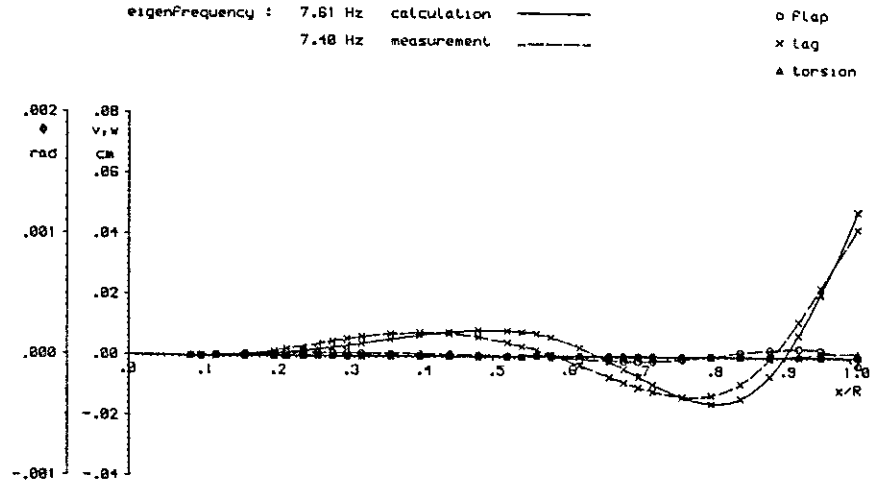

Figure 9: 3rd Lag Mode of the Rotor Blade

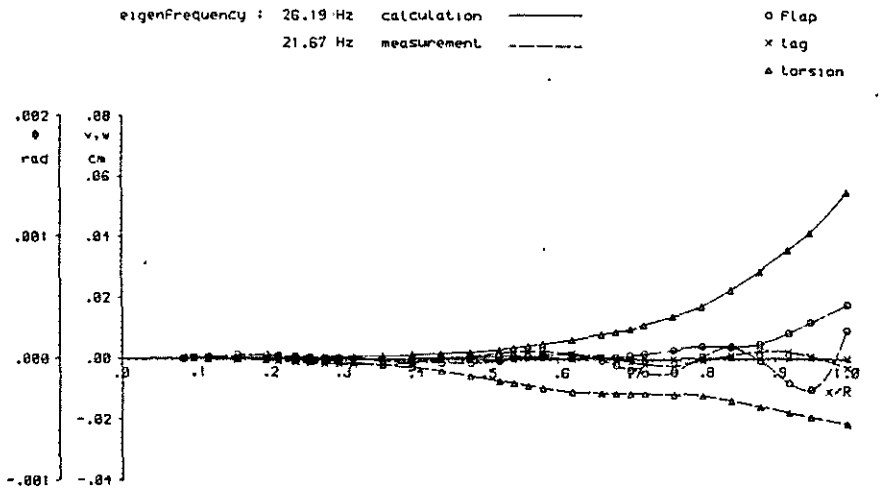

Figure 10: 1st Torsion Mode of the Rotor Blade

$\underline{\bar{M}}_{CC}$

	F1	F2	F3	F4	F5	F6	F7	L1	L2	L3	L4	L5	T1	
F1	100.0													F1
F2	0.0	100.0												F2
F3	0.0	0.0	100.0											F3
F4	0.0	0.0	0.0	100.0										F4
F5	0.0	0.0	0.0	0.0	100.0									F5
F6	0.0	0.0	0.0	0.0	0.0	100.0								F6
F7	0.0	0.0	0.0	0.0	0.0	0.0	100.0							F7
L1	0.0	0.0	0.0	0.0	0.0	0.0	0.0	100.0						L1
L2	0.0	0.0	0.0	0.0	0.0	0.0	0.0	0.0	100.0					L2
L3	0.0	0.0	0.0	0.0	0.0	0.0	0.0	0.0	0.0	100.0				L3
L4	0.0	0.0	0.0	0.0	0.0	0.0	0.0	0.0	0.0	0.0	100.0			L4
L5	0.0	0.0	0.0	0.0	0.0	0.0	0.0	0.0	0.0	0.0	0.0	100.0		L5
T1	0.0	0.0	0.0	0.0	0.0	0.0	0.0	0.0	0.0	0.0	0.0	0.0	100.0	T1
	F1	F2	F3	F4	F5	F6	F7	L1	L2	L3	L4	L5	T1	

$\underline{\bar{M}}_{MC}$

	F1	F2	F3	F4	F5	F6	F7	L1	L2	L3	L4	L5	T1	
F1	[-99.9]	1.9	4.4	-1.5	0.3	-0.3	-0.5	0.0	0.0	0.0	0.0	0.0	-0.4	F1
F2	-5.1	[-98.4]	-12.2	7.8	5.4	-4.2	3.7	0.0	0.0	0.0	0.0	0.0	-0.9	F2
F3	6.0	-17.6	[94.4]	-22.5	-10.3	6.1	-2.1	0.2	6.9	4.8	3.3	0.3	-0.2	F3
F4	2.0	6.8	33.2	[85.2]	27.2	-15.7	11.2	-2.9	6.0	-12.1	-7.1	-3.1	-1.3	F4
F5	4.5	-5.6	-11.4	46.0	[-76.0]	33.5	-13.8	1.3	-2.1	4.8	-13.2	1.5	0.9	F5
F6	-1.3	3.4	4.6	-15.4	-54.7	[-69.4]	35.1	0.6	-1.1	0.7	-3.6	5.9	-2.3	F6
F7	-0.7	1.6	11.2	-9.1	-8.6	47.8	[62.1]	0.3	5.3	5.5	8.6	10.2	24.1	F7
L1	0.0	0.0	0.0	0.0	0.0	0.0	0.0	[99.1]	-12.2	-5.6	-0.8	0.3	0.0	L1
L2	-2.1	-5.5	-0.5	-2.0	-3.4	2.4	-1.7	5.6	[96.4]	20.9	9.4	6.6	0.2	L2
L3	-1.4	-4.2	0.7	-11.7	-3.5	3.0	-2.0	-2.7	23.7	[-90.7]	-27.4	-13.3	-0.4	L3
L4	0.5	-2.7	3.3	9.7	-8.6	4.8	-2.5	-1.2	-9.0	-44.3	[77.3]	36.9	-1.2	L4
L5	-0.5	-1.3	2.3	3.8	-6.6	1.7	2.2	-4.4	3.0	5.1	65.7	[-59.1]	1.2	L5
T1	-4.9	0.8	0.2	0.3	-2.6	-18.0	-8.9	2.4	-1.2	-1.0	5.4	19.8	[78.9]	T1
	F1	F2	F3	F4	F5	F6	F7	L1	L2	L3	L4	L5	T1	

$\underline{\bar{M}}_{MM}$

	F1	F2	F3	F4	F5	F6	F7	L1	L2	L3	L4	L5	T1		Δ
F1	100.0													F1	992
F2	2.5	100.0												F2	988
F3	-2.0	2.8	100.0											F3	981
F4	-1.7	-1.0	6.5	100.0										F4	984
F5	-5.9	3.3	-9.6	5.2	100.0									F5	967
F6	1.5	-2.7	7.2	-8.2	1.5	100.0								F6	955
F7	0.4	-1.9	[14.8]	-2.5	-1.1	6.0	100.0							F7	952
L1	0.0	0.0	-0.9	-2.9	1.4	0.8	-0.7	100.0						L1	925
L2	2.0	4.9	9.4	-2.0	1.5	-1.8	6.8	-7.3	100.0					L2	920
L3	1.6	2.6	1.0	2.3	-1.7	-1.1	-9.0	-0.3	0.9	100.0				L3	973
L4	-0.5	2.1	2.7	4.1	1.6	-1.9	7.7	2.3	-6.9	10.3	100.0			L4	991
L5	0.4	1.1	4.6	-1.2	-2.9	-3.0	3.8	-6.6	3.9	-11.8	[19.0]	100.0		L5	978
T1	4.5	-1.7	-0.5	-1.9	-0.8	8.9	6.0	2.6	1.4	-3.8	11.3	-9.4	100.0	T1	946
	F1	F2	F3	F4	F5	F6	F7	L1	L2	L3	L4	L5	T1		

Table 2: Submatrices of the Correlation Matrix

The correlation between the calculated and the measured eigenmodes can be taken from the diagonal elements of the matrix $\underline{\bar{M}}_{MC}$. There is a correlation of over 90 % for the first three flap and lag modes. In the higher bending modes and in the torsion mode the conformity is not so good. The difference between the calculated and measured mode shapes is obvious. The area of

the clamping device appears to be assumed too stiff in the FE-calculations. In this area the measured higher eigenmodes have greater components as the calculated ones and, as mentioned, coupling does not occur in the calculations contrary to the measurement. The results of FE-calculations can be only as good as the input data, as regards the mass and stiffness distributions.

7. Conclusions

A computer program for the free vibration analysis of rotor blades was developed by application of the finite element method. The formulation was made for coupled bending and torsion of a twisted nonuniform rotor blade. The blade was assumed to be structurally symmetric about the major principle axis. There were no restrictions concerning the geometric arrangement of the elastic, neutral, and mass axes.

The analytical deduction of the mass and stiffness matrices of the finite rotor beam element was performed by a non-numeric computer program. With this programm it was possible to weight the variables and to simplify the derivation in a systematic manner.

The finite element calculations, performed for a nonrotating homogeneous beam, yielded good results. There were only small differences between the eigenfrequencies end eigenmodes of the analytical solution and the FE-calculations. As another example, the FE-calculations were carried out for an actual rotor blade of a wind energy converter. This blade was investigated in a ground vibration test and the modal parmeters were determined. The comparision of the measured and computed smallest flap and lag natural mode shapes and frequencies was very satisfactory. Greater differences occured at the higher modes.

Finally, it must to be mentioned, that the results permit no conclusions as regards a creditable specification of the influence of the twist and the tension in the FE-formulation. A twisted rotating blade should be investigated in a vibration test to prove this influence. The blade should be built very simple, so that the cross section constants could be calculated easily. It could be examined how the test results are compatible with the finite element model.

8. References

1. J.C. Houbolt, G.W. Brooks — Differential Equations of Motion for Combined Flapwise Bending, Chordwise Bending, and Torsion of Twisted Nonuniform Rotor Blades. NACA Rep. 1346, 1958.

2. H.W. Försching — Dynamische und aeroelastische Probleme des Stop-Rotors und ihre analytische Behandlung. Teil I : DLR-FB 72-65 (1972). Teil II: DLR-FB 73-19 (1973).

3. D.H. Hodges, R.A. Ormiston — Nonlinear Equations for Bending of Rotating Beams with Application to Linear Flap-Lag Stability of Hingeless Rotors. NASA TM X-2770, May 1973.

4. D.H. Hodges, E.H. Dowell — Nonlinear Equations of Motion for the Elastic Bending and Torsion of Twisted Nonuniform Rotor Blades. NASA TN D-7818, Dec. 1974.

5. D. Petersen — Nichtlineare Transformationsmatrix für den gedehnten, gebogenen und tordierten Stab. DLR-FB 76-62 (1976).

6. K.R.V. Kaza, R.G. Kvaternik — Nonlinear Flap-Lag-Axial Equations of a Rotating Beam. AIAA Journal, Vol. 15, No. 6, June 1977, pp. 871-874.

7. P.P. Friedmann — Recent Developments in Rotary-Wing Aeroelasticity. J. Aircraft, Nov. 1977, pp. 1027-1041.

8. K.R.V. Kaza, R.G. Kvaternik — Nonlinear Curvature Expressions for Combined Flapwise Bending, Chordwise Bending, Torsion, and Extension of Twisted Rotor Blades. NASA TM X-73997, Dec. 1976.

9. K.R.V.Kaza, R.G. Kvaternik — Nonlinear Aeroelastic Equations for Combined Flapwise Bending, Chordwise Bending, Torsion, and Extension of Twisted Nonuniform Rotor Blades in Forward Flight. NASA TM 74059, Aug. 1977.

10. K.R.V. Kaza, R.G. Kvaternik, W.F. White, Jr. — Nonlinear Flap-Lag-Axial Equations of a Rotating Beam with Arbitrary Precone Angle. AIAA Paper 78-491, Proceedings of AIAA/ASME 19th Structures, Structural Dynamics and Material Conference, Bethesda, Maryland, April 1978, pp. 214-227.

11. D. Petersen — Möglichkeiten und Grenzen der Stabtheorien. DFVLR-FB 78-13 (1978).

12. P.P. Friedmann, F. Straub — Application of the Finite Element Method to Rotary-Wing Aeroelasticity. Paper No. 24, Proceedings of the Fourth European Rotorcraft and Powered Lift Forum, Stresa, Italy, Sept. 1978.

13. D. Petersen — Ein Beitrag zur nichtlinearen Stabtheorie. ZAMM 59 (1979), T 205 - T 206, 1979.

14. D.H. Hodges, R.A. Ormiston, D.A. Peters — On the Nonlinear Deformation Geometry of Euler-Benoulli Beams. NASA TP 1566, Apr. 1980.

15. A. Rosen — The Effect of Initial Twist on the Torsional Rigidity of Beams - Another Point of View. Journal of Applied Mechanics, Vol. 47 (1980), pp. 389-392.

16. D.H. Hodges — Torsion of Pretwisted Beams Due to Axial Loading. Journal of Applied Mechanics, Vol. 47, (1980), pp. 393-397.

17. D. Petersen — Interaction of Torsion and Tension in Beam Theory. Paper No. 20, Proceedings of the Sixth European Rotorcraft and Powered Lift Forum, Bristol, Sept. 1980.

18. N.T. Sivaneri, I. Chopra — Dynamic Stability of a Rotor Blade Using Finite Element Analysis. AIAA Paper No. 81-0615, Proceedings Part II of the 22nd Structures, Structural Dynamics and Materials Conference, Atlanta, Georgia, 6.-8.4.1981.

19. F. Kießling, D. Ludwig — Berechnung der Eigenschwingungen von Rotorblättern mit der Methode der finiten Elemente. DFVLR-FB 81-07 (1981).

20. E. Breitbach — A Semi-Automatic Modal Survey Test Technique for Complex Aircraft and Spacecraft Structures. ESRO SP-99, Proceedings of the Third Testing Symposium, Frascati, Italy, 22.-26.10.73.

21. E. Breitbach, M. Degener, N. Niedbal — Modal Survey ESA SP-121, Lectures and Discussions Held at ESTEC, Nordwijk, Netherlands, 5.-6.10.76.

22. N. Niedbal — Obtaining Normal Mode Parameters From Modal Survey Tests. Preprint IAF-79-f-199, XXX. Congress International Astronautical Federation, Munich, FRG, 17.-22.9.79.

Appendix A

The transformation matrices $\underline{\underline{T}}_0$ and $\underline{\underline{T}}_1$ are defined by:

$$\underline{\underline{T}}_0 = \begin{bmatrix} 1 & 0 & 0 \\ 0 & \cos\beta & -\sin\beta \\ 0 & \sin\beta & \cos\beta \end{bmatrix},$$

and

$$\underline{\underline{T}}_1 = \left[\begin{array}{cc|ccc|ccc} \cos\alpha_1 & \cos\alpha_2 & & -\sin\alpha_1 & \cos(\beta+\phi) & & \sin\alpha_1 & \sin(\beta+\phi) \\ & & & -\cos\alpha_1 & \sin\alpha_2 \sin(\beta+\phi) & & -\cos\alpha_1 & \sin\alpha_2 \cos(\beta+\phi) \\ \hline \sin\alpha_1 & \cos\alpha_2 & & \cos\alpha_1 & \cos(\beta+\phi) & & -\cos\alpha_1 & \sin(\beta+\phi) \\ & \sin\alpha_2 & & -\sin\alpha_1 & \sin\alpha_2 \sin(\beta+\phi) & & -\sin\alpha_1 & \sin\alpha_2 \cos(\beta+\phi) \\ \hline & \sin\alpha_2 & & \cos\alpha_2 & \sin(\beta+\phi) & & \cos\alpha_2 & \cos(\beta+\phi) \end{array}\right],$$

where

$$\sin\alpha_1 = \frac{v'}{\sqrt{1 + v'^2}},$$

$$\cos\alpha_1 = \frac{1}{\sqrt{1 + v'^2}},$$

$$\sin\alpha_2 = \frac{w'}{\sqrt{1 + v'^2 + w'^2}},$$

$$\cos\alpha_2 = \frac{\sqrt{1 + v'^2}}{\sqrt{1 + v'^2 + w'^2}}.$$

The trigonometrical functions with the arguments α_1 and α_2 as well as those with the elastic torsion ϕ can be expanded into series. If all terms greater than $O(\varepsilon^2)$ are neglected this yields:

$$\sin\alpha_1 \approx v' \left(1 - \frac{1}{2} v'^2\right) \approx v',$$

$$\cos\alpha_1 \approx 1 - \frac{1}{2} v'^2,$$

$$\sin\alpha_2 \approx w' \left(1 - \frac{1}{2} v'^2 - \frac{1}{2} w'^2\right) \approx w',$$

$$\cos\alpha_2 \approx \left(1 + \frac{1}{2} v'^2\right) \left(1 - \frac{1}{2} v'^2 - \frac{1}{2} w'^2\right) \approx 1 - \frac{1}{2} w'^2,$$

$$\sin\Phi \approx \phi - \frac{1}{6} \phi^3,$$

$$\cos\Phi \approx 1 - \frac{1}{2} \phi^2 + \frac{1}{24} \phi^4.$$

Appendix B

The strain tensor components and the components of the absolute velocity vector were calculated by neglecting all terms greater than $O(\varepsilon^2)$:

$$\varepsilon_{xx} = u' + \frac{1}{2} v'^2 + \frac{1}{2} w'^2 - \lambda \Phi'' + (\eta^2 + \zeta^2) (\beta' \Phi' + \frac{1}{2} \Phi'^2) -$$

$$- \eta (v'' \cos\beta + w'' \sin\beta) + \eta \Phi (v'' \sin\beta - w'' \cos\beta) +$$

$$+ \zeta (v'' \sin\beta - w'' \cos\beta) + \zeta \Phi (v'' \cos\beta + w'' \sin\beta),$$

$$\gamma_{x\eta} = - (\zeta + \lambda_\eta) \Phi' ,$$

$$\gamma_{x\zeta} = (\eta - \lambda_\zeta) \Phi' ;$$

and

$$v_{1,X} = \dot{u} - \lambda \dot{\Phi}' + \dot{\Phi} [v' (\zeta \cos\beta + \eta \sin\beta) + w' (\zeta \sin\beta - \eta \cos\beta)] +$$
$$+ \Omega [(\Phi - \frac{1}{6} \Phi^3) (\zeta \cos\beta + \eta \sin\beta) + (1 - \frac{1}{2} \Phi^2) (\zeta \sin\beta - \eta \cos\beta) - v - e_0],$$

$$v_{1,Y} = \dot{v} + \dot{\Phi} [\Phi (\zeta \sin\beta - \eta \cos\beta) - (1 - \frac{1}{2} \Phi^2) (\zeta \cos\beta + \eta \sin\beta)] +$$
$$+ \Omega [(\Phi w' + v') (\zeta \sin\beta - \eta \cos\beta) + (\Phi v' - w') (\zeta \cos\beta + \eta \sin\beta) +$$
$$+ u + x - \lambda \Phi'],$$

$$v_{1,Z} = \dot{w} - \dot{\Phi} [(1 - \frac{1}{2} \Phi^2) (\zeta \sin\beta - \eta \cos\beta) + \Phi (\zeta \cos\beta + \eta \sin\beta)] .$$

If all terms of the order greater than $O(\varepsilon^4)$ are ignored the potential energy results in:

$$U = \frac{1}{2} \int_0^R [EI_1 (v'' \sin\beta - w'' \cos\beta)^2 + EI_2 (v'' \cos\beta + w'' \sin\beta)^2 +$$
$$+ (GJ + EB_1 \beta'^2) \Phi'^2 - 2EB_2 (v'' \cos\beta + w'' \sin\beta) \beta' \Phi' +$$
$$+ EC_1 \Phi''^2 - 2 EC_2 (v'' \sin\beta - w'' \cos\beta) \Phi'' + \frac{T^2}{EA}] dx .$$

In the equation for the kinetic energy all terms greater than $O(\varepsilon^3)$ are neglected:

$$
\begin{aligned}
V = & \int_0^R \Omega^2 \, m \, x \, u \, dx + \\
& + \int_0^R \Omega^2 \, m \, \{e \, x \, [\Phi \, (v' \sin\beta - w' \cos\beta) - (v' \cos\beta + w' \sin\beta)] + \\
& + v \, (e \cos\beta + e_0 - e \, \Phi \sin\beta) + \frac{1}{2} v^2 + \\
& + \Phi \, [(k_{m1}^2 - k_{m2}^2) \sin\beta \cos\beta - e \, e_0 \sin\beta] + \\
& + \frac{1}{2} \Phi^2 \, [(k_{m1}^2 - k_{m2}^2) \cos 2\beta - e \, e_0 \cos\beta] + \\
& + \frac{1}{6} \Phi^3 \, e \, e_0 \sin\beta + \\
& + \frac{1}{2} (x^2 + e_0^2 + 2 \, e \, e_0 \cos\beta + k_{m1}^2 \sin^2\beta + k_{m2}^2 \cos^2\beta)\} \, dx + \\
& + \int_0^R \Omega \, m \, \{- \dot{u} \, e_0 + \dot{v} \, x + \dot{\Phi} \, [e \, x \, (\tfrac{1}{2} \Phi^2 \sin\beta - \Phi \cos\beta + \sin\beta) - \\
& - e \, e_0 \, (v' \sin\beta - w' \cos\beta)]\} \, dx + \\
& + \int_0^R m \, [\tfrac{1}{2} (\dot{v}^2 + \dot{w}^2 + k_m^2 \dot{\Phi}^2) - e \, \dot{\Phi} \, (\dot{v} \sin\beta - \dot{w} \cos\beta)] \, dx ,
\end{aligned}
$$

where

$$
\begin{aligned}
\int_0^R \Omega^2 \, m \, x \, u \, dx = \int_0^R T \, u' dx = \int_0^R T \, [\tfrac{T}{EA} - \tfrac{1}{2} (v'^2 + w'^2) - \\
- k_A^2 (\Phi' \beta' + \tfrac{1}{2} \Phi'^2) + e_A (v'' \cos\beta + w'' \sin\beta) - \\
- e_A \Phi (v'' \sin\beta - w'' \cos\beta)] \, dx .
\end{aligned}
$$

These equations are obtained in considering the following section integrals:

$$A = \int_A dA \quad , \; O(\varepsilon) \qquad k_A^2 A = \int_A (\eta^2 + \zeta^2) dA \quad , \; O(\varepsilon^2)$$

$$e_A A = \int_A \eta dA \quad , \; O(\varepsilon^{3/2}) \qquad J = \int_A [(\eta - \lambda_\zeta)^2 + (\zeta + \lambda_\eta)^2] dA, \; O(\varepsilon^2)$$

$$I_1 = \int_A \zeta^2 dA, \; O(\varepsilon^2) \qquad I_2 = \int_A \eta^2 dA - e_A^2 A \quad , \; O(\varepsilon^2)$$

$$C_1 = \int_A \lambda^2 dA, \; O(\varepsilon^3) \qquad B_1 = \int_A (\eta^2 + \zeta^2 - k_A^2)^2 dA \quad , \; O(\varepsilon^3)$$

$$C_2 = \int_A \lambda\zeta dA, \; O(\varepsilon^{5/2}) \qquad B_2 = \int_A \eta \, (\eta^2 + \zeta^2 - k_A^2) dA \quad , \; O(\varepsilon^{5/2})$$

and

$$m = \int_A \rho \, dA \quad , \; 0(\varepsilon)$$

$$k_{m1}^2 \, m = \int_A \rho \, \zeta^2 \, dA, \; 0(\varepsilon^2)$$

$$em = \int_A \rho \, \eta \, dA, \; 0(\varepsilon^{3/2})$$

$$k_{m2}^2 \, m = \int_A \rho \, \eta^2 \, dA, \; 0(\varepsilon^2)$$

$$k_m^2 = k_{m1}^2 + k_{m2}^2$$

On the assumption of a symetrical cross section of the rotor blade these integrals will become zero:

$$\int_A \zeta(\eta^2 + \zeta^2)dA = 0$$

$$\int_A \zeta dA = 0$$

$$\int_A \lambda(\eta^2 + \zeta^2)dA = 0$$

$$\int_A \eta\zeta dA = 0$$

$$\int_A \lambda\eta dA = 0$$

$$\int_A \lambda dA = 0$$